**ORIGINAL PAPER**

# Estimation of flood inundation in river basins of Uttar Pradesh using Sentinel 1A-SAR data on Sentinel Application Platform (SNAP)

Pawan Kumar Gautam[1] · Sushil Chandra[1] · Pradnita Komal Henry[1]

## Abstract

Severe flood events during the last decades have proved to be a devastating disaster for the densely populated and economy of Uttar Pradesh. Due to its ability to provide a concise view of spatial extent of the flood, remote sensing techniques and synthetic aperture radar (SAR) systems in particular have been applied to flood mapping. The present study has identified flood-prone areas in Uttar Pradesh using the C-band (SAR) sensor of Sentinel-1. In this study, changes in flood inundation area during the monsoon season of 2021 have been estimated. Sentinel Application Platform (SNAP) has been used to perform SAR pre-processing which includes orbit file application, thermal noise removal, calibration, speckle filtering, and terrain correction. Subsequently, polarization, band math expression, thresholding, and image are processed. In addition, image mapping has been done in Arc-GIS tool for detailed investigation of flood inundation area. Detailed investigation of the flood inundated area found that overall, 7710 km$^2$ is affected by the flood area. This study will be the potential use of microwave SAR remote sensing as a comprehensive and effective way of providing accurate surface water information for water resources management, flood warning, flood monitoring, and rapid and accurate flood damage assessment in the years to come.

**Keywords** Flood inundation mapping · Synthetic aperture radar · Sentinel 1 · Threshold · Uttar Pradesh

## Introduction

Flood is a natural disaster that is most devastating and frequent occurring natural disaster in the world, leading to loss of life and property each year. Uttar Pradesh is a largest state by crop land area, and most populous state of India. The landscape of the region is characterized by flat surface and cropland formed by the Ganges River and its tributaries. Many areas are prone to severe flooding during the monsoon season, resulting large annual losses. The land along the

channel in the valley is recognized as the floodplain of the river. This area is considered most sensitive from flood point of view (Gautam and Singh 2022).

Flood is one type of natural hazard which adversely affects the society and environment every year (Singh and Awasthi 2011). It causes great devastation and damage to life and property (Li et al. 2019). The risk of a flood may arise during a period at a given time and place (Gautam et al. 2022b; Varnes 1984). Based on the assessment of the Central Water Committee, about 37 million hectares, which is about 1/8th of the fertile geographical area of India, this part is vulnerable to floods during monsoon (Valdiya 2004). Many countries are affected due to floods; therefore, it has been listed as a natural disaster in the world (Ogah et al. 2013). The unconsolidated material is also responsible for flooding in Uttar Pradesh (Gautam et al. 2023).

Due to frequent flood events, erosion and siltation in the river banks increase, which has a negative impact on agriculture or soil fertility (Chutiya et al. 2009). Floods alone affected 2.3 billion people worldwide during 1998–2015 (Wallemacq et al. 2015). Around 21 million people worldwide are affected by floods annually, which may increase

✉ Pawan Kumar Gautam
geopawan9@gmail.com

Sushil Chandra
schandra.77653@gov.in

Pradnita Komal Henry
pradnitapioneer19@gmail.com

1 Remote Sensing Applications Centre, Uttar Pradesh, Department of Science & Technology, Lucknow, Govt. of U.P., India

to 54 million by 2030 due to climate change and socio-economic development (Luo et al. 2015). The Ganga Basin is the most vulnerable region to climate change due to its dense population and high dependence on agriculture (Khan et al. 2018). The sediment load of the Ganges–Brahmaputra delta is the largest in the world covering an area of 1.76 million $km^2$ (Rudra 2014). Each year, floods deposit about 1060 m of sediment into the Indian Ocean through the Ganges–Brahmaputra delta, which is one of the largest river sediment deposits in the world (Milliman and Farnsworth 2011).

The impact of climate change and associated hazards on the rivers (typically for flooding) has been investigated by (Kumar et al. 2018; Singh 2007, 2010, 2013, 2015), in himalayan region (Singh et al. 2019; Singh et al. 2022; Gautam and Singh 2023; Kumar et al. 2024), in Peninsular India (Gautam 2023a). There is a risk of flooding during high discharge periods (Singh and Awasthi 2011). During heavy rains, the behavior of the river basin becomes abnormal, due to which the risk of flood increases (Perucca and Angilieri 2010; Singh et al. 2015). Unplanned rapid urbanization, land use/land cover change, and inadequate wetland management are becoming important issues to consider especially in flood plains (Adelekan 2011).

Sentinel-1A was launched through the Global Monitoring for Environment and Security (GMES) program on April 3 (European Space Agency 2016). As a synthetic aperture radar (SAR) satellite, Sentinel-1A uses C-band wavelength to record objects on the land with a frequency between 5250 and 5570 MHz (Torres et al. 2012) and produces two main products, namely, slant range, single-look complex (SLC), and ground range detection (GRD) (European Space Agency 2016).

Due to the high penetration capability of synthetic aperture radar (SAR) dataset, it can be used to detect floods in vegetated or urban areas (Mason et al. 2012). SAR data has been preferred to locate flood affected areas over optical data due to its atmospheric capabilities to operate in all-weather conditions throughout day/night time and can potentially penetrate through clouds, haze, fog, smog, heavy rain, moist, etc., (Joyce et al. 2009; Manavalan 2017; Patel et al. 2009). Following the successful launch of the first space-borne SAR sensor on board ERS-1 in 1991, significant research was conducted into effectively using SAR data for uninterrupted flood monitoring (Bhatt et al. 2013; Bolanos et al. 2016; Rahman and Thakur 2017). Active microwave sensors and synthetic aperture radars are suitable for flood mapping due to their ability to provide observations in all conditions regardless of adverse illumination and weather conditions (Singh et al. 2018; Tavus and Kocaman 2022). In radar remote sensing, the incident signal undergoes specular reflection which results in less backscatter when soil water content exceeds

50% (Srivastava et al. 2006). Several researchers have proposed techniques to automatically characterize open water based on the binarization nature of SAR backscatter histograms over dense terrain (Sezgin and Sankur 2004; Fan and Lei 2012). Earlier studies show that SAR datasets were preferentially used for mapping and monitoring flood extent (Zwenzner 2009; Voormansik et al. 2014; Greifeneder et al. 2014; Rahman and Thakur 2018; Uddin et al. 2019, Li et al. 2019). The potential use of microwave SAR for monitoring and mapping of flood inundated areas was followed by various researchers (Amitrano et al. 2018; Nasirzadehdizaji et al. 2019; Meyer et al. 2022; Abazaj Hasko 2020; Tavus et al. 2018; Vanama et al. 2021; Karamvasis 2021).

SAR-based flood mapping techniques include manual or automatic threshold (Manjusree et al. 2012; Martinis et al. 2015). Detected by thresholding SAR data to map the extent of flooding in the Caprivi flood zone (Long et al. 2014). Threshold-based techniques are used in SAR to detect and monitor floods (Pradhan et al. 2016). Threshold-based methods are most commonly used for flood detection and provide reliable results in real-time mapping (Amitrano et al. 2018). The capability of C-band Sentinel-1 SAR data of VV and VH polarization is adopted as threshold technique to extract the river extent (Pham-Duc et al. 2017; Sivasankar et al. 2019).

Maps of flood affected area and flood frequency should be prepared to alert and protect people (Singh et al. 2018). Flood maps can be useful for populations to help prevent flood risks (Demir and Kisi 2016). In this context, remote sensing (RS)–based data provides

**Table 1**  Major rivers of Uttar Pradesh showing average annual flows at various gauging points/ tributaries in million cubic meters and discharge ($m^3$/s) is given below

| River | Station | Average annual flows (million cubic meter) | Discharge ($m^3$/s) |
|---|---|---|---|
| Ganga | Haridwar | 23,900 | 11,470 |
|  | Narora | 31,400 |  |
|  | Allahabad | 58,980 |  |
| Yamuna | Allahabad | 93,020 | 2950 |
|  | Tajewala | 10,750 |  |
|  | Delhi | 13,700 |  |
| Ghaghara | Ganga confluent | 94,400 | 2990 |
| Gandak | Ganga confluent | 52,200 | 2025 |
| Gomati | Ganga confluent | 7390 | 234 |
| Betwa | Yamuna confluent | 10,000 | 658 |
| Chambal | Yamuna confluent | 30,050 | 456 |
| Ken | Yamuna confluent | 11,300 | 310 |
| Sind | Yamuna confluent | 700 | 290 |

(Source: Water Resource Information System (WRIS), India)

**Table 2** Some sensors used for flood mapping studies

| Data | Version/scale | Source |
|---|---|---|
| Arc-GIS | v.10.4.1 | https://rsac.up.gov.in |
| Erdas Imagine | 2014 | https://hexagon.com/products/erdas-imagine |
| Sentinel 1A (GRD) | 5×20 Sq. m | https://scihub.copernicus.eu/dhus/#/home |
| SNAP tool | v.8.0.9 | https://step.esa.int/main/download |
| Boundary | Vector | https://www.nrsc.gov.in |
| SRTM (DEM) | 90 m | https://cgiarcsi.community/data/srtm-90m-digital-elevation-database-v4-1 |

multi-resolution satellite data for flood mapping and identifying flood-prone areas, which is the first step for formulating any flood management strategy (Sahoo and Sreeja 2017). Data has been collected from each hydrological station located in the drainage basin (Table 1). Due to its characteristics (relief, hydrology, climatology), the Ganga Basin is definitely one of the most exposed due to its vulnerability; the valleys are prone to flood natural environment that is most vulnerable and the area most at risk for erosion and flooding.

Since the Ganga plain is located in the foothills of the Himalayas, it is the region with the highest rainfall in low-lying northern India, causing severe, unprecedented flooding during the monsoon season (Nandargi and Shelar 2018). The states facing the most floods are Uttar Pradesh, Bihar, and West Bengal. The frequency of floods was measured to be lowest in the years 1992, 2009, 2012, 2014, and 2015, while it was highest in the years 1987, 1998, 1999, 2001, 2003, and 2013 (Nandargi and Shelar, 2018) (Table 1). Major Rivers of Uttar Pradesh show average annual flows at various gauging points in million cubic meters and
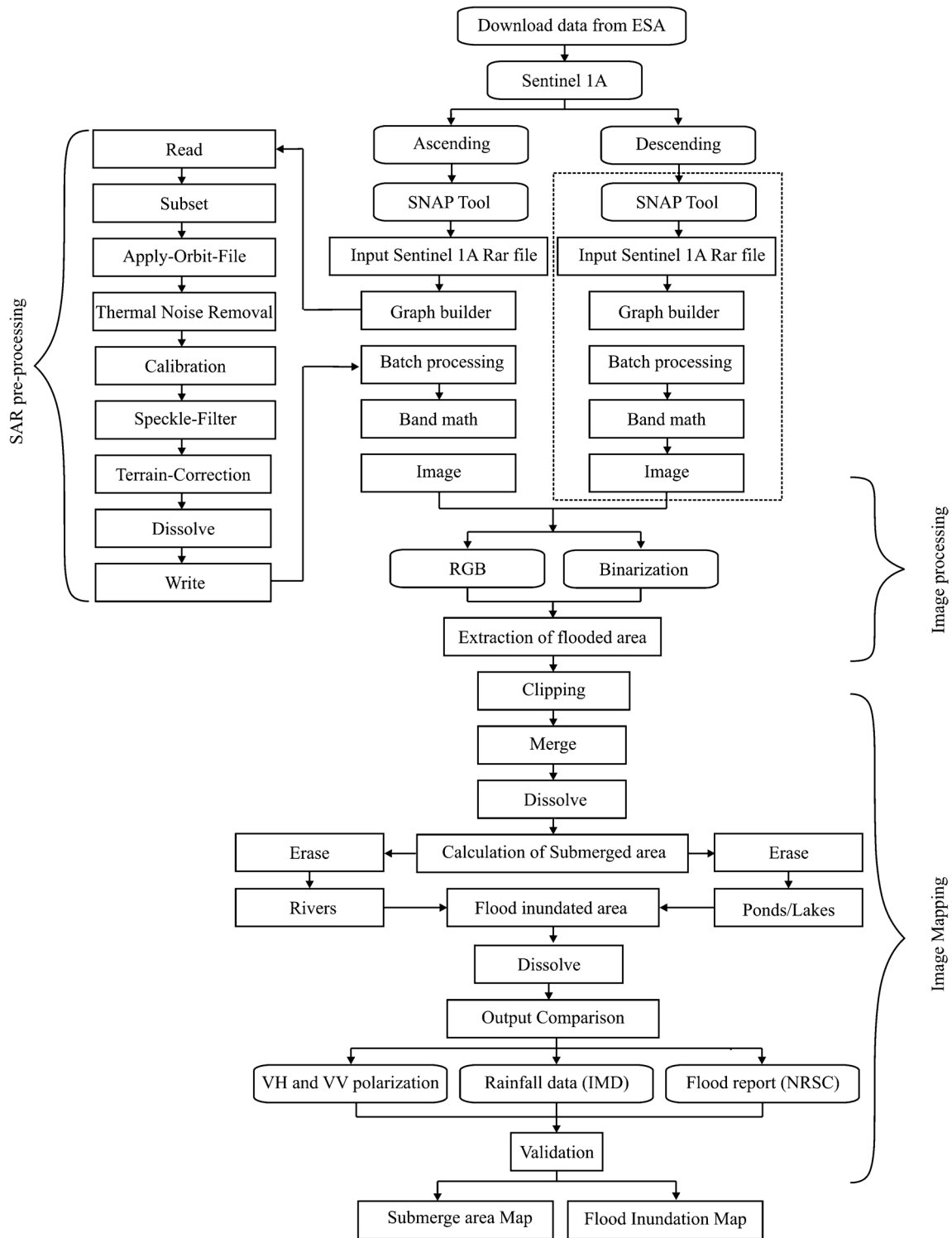


**Fig. 1** Study area
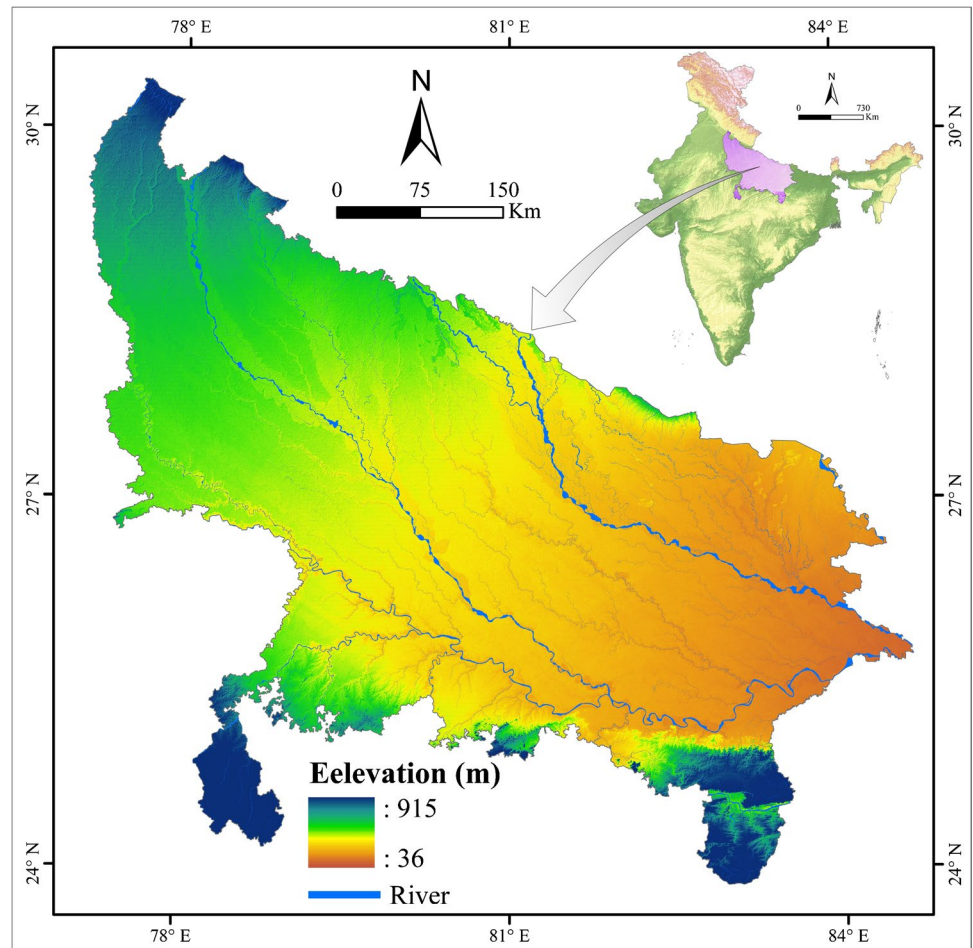
**Fig. 2** Outline of the methodology

discharge (m³/s) of each hydrological station (Table 2). Due to relief, hydrology, and climatology, the Ganges basin is undoubtedly the most exposed due to its vulnerability, with the valleys most prone to erosion and flooding due

to which most of the region come under vulnerable condition. Currently, there is reliance on traditional flood study and assessment knowledge, but satellite data can now help in flood mapping and identifying flood-prone areas for a

**Table 3** The area submerged during different dates in the monsoon season

| Months | Submerged area (km$^2$) | | | Flood inundated area (km$^2$) | | Seasons |
|---|---|---|---|---|---|---|
| | Ascending | Descending | Submerged area (km$^2$) dissolve | Flood inundated area | After clip lake/ponds | |
| Jun | 4390 | 3532 | 4088 | - | - | Monsoon |
| Jul | 3722 | 4067 | 4696 | 1521 | 1241 | Monsoon |
| Aug | 7422 | 6518 | 8793 | 5382 | 4935 | Monsoon |
| Sept | 6766 | 5417 | 7756 | 4337 | 3828 | Monsoon |
| Oct | 6754 | 5745 | 7955 | 4374 | 3909 | Post-monsoon |
| Total flood inundated area along the river | | | | | | 7710 km$^2$ |

more adequate understanding of flood events and other river hazards. Sentinel-1 SAR-based flood maps have provided an accuracy of 96.44% in Bangladesh (Uddin and Matin 2019). Geospatial techniques such as open-access Sentinel-1 data provide immediate assessment for flood disaster.

In this scenario, the present work followed by objectives to identify flood-prone areas in Uttar Pradesh using Sentinal 1A SAR data. Identification of flood zones will provide insight into changes in flood zones and predict potential flood encroachment for pre- and post-disaster change detection scenarios. This technology provides reliable and accurate discrete disaster risk maps and emergency management. The objective of this research is to characterize the flooded area using simple techniques that bring to the fore freely available SAR data.

## Study area

Uttar Pradesh is a state in northern part of India. Geographically, the study area extends over 23°42′47.648″N to 30°40′51.887″N latitudes and 76°28′53.854″E to 84°58′15.51″E longitudes, and the elevation is 36–900 m above mean sea level (Fig. 1). The climate is mainly subtropical humid with 794 mm of annual rainfall. In general, the rainfall intensity is declined from east to west; it receives high to moderate rainfall from June to September during monsoon season, respectively. Heavy rain during monsoon season causes catastrophic flood in the low-lying areas of

the Uttar Pradesh (Kumar et al. 2018). The highest temperature is recorded during month of June, reaching up to 47 °C, while winter season records that temperature varies between 2 and 20 °C (Kumar and Singh 1978; Sinha 2005, Gautam 2023b). The outlying area typically receives mean annual rainfall from 80 to 160 cm (Jain and Sinha 2003; Sinha et al. 2005) during the monsoon season (June–September). Four distinct seasons can be adequately recognized, i.e., summer, monsoon, and winter (Singh 1988). They often occur from west and northwest between October and April, and from May, it shifts east and southeast during the southwest monsoon season (Singh et al. 2018; Gautam et al. 2020, 2022a, 2022b, 2023; Gautam and Singh 2022). The area exhibits a gentle southward slope and the elevation range between 36 and 915 m (amsl). Total area is around 240,939 km$^2$, and the total population accounts is approximately 231,502,578.

## Data acquisition

In this study, time-series data from the Sentinel Application Platform (SNAP) platform has been employed for data processing and identification of flood-prone areas in Uttar Pradesh. The study uses the Interferometric Wide-Swath (IW) acquisition mode at the level of Ground Range Detected (GRD) with 250 km swath range with 5×20 sq. m spatial resolution, which is available in VV (vertical–vertical) and VH (vertical-horizontal) dual polarization (European Space Agency 2016). The open-access SNAP (v.8.0.9) toolbox is

**Table 4** Statistics for classified and photo-interpretation flood water areas

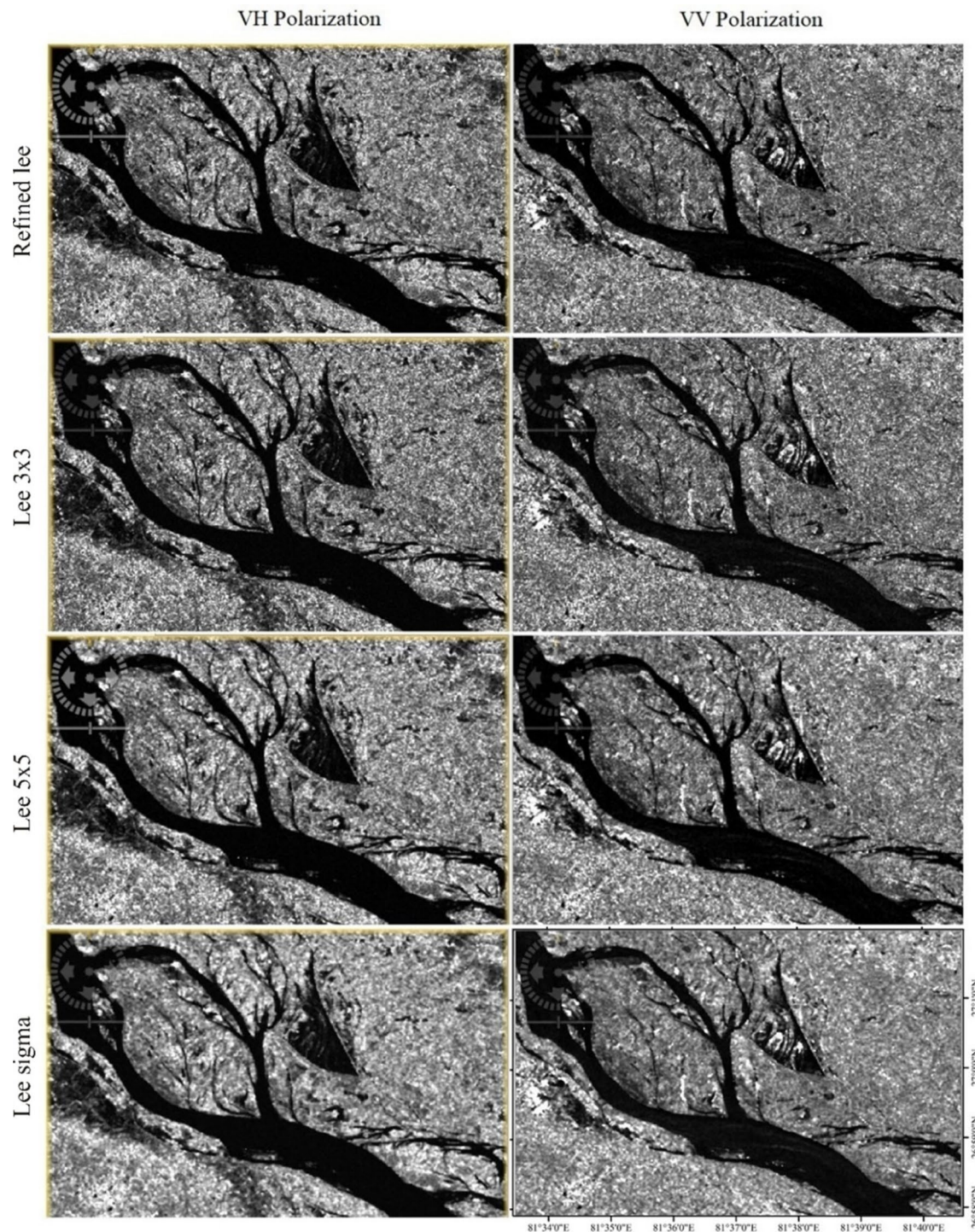| Sites | Area (ha) | | | | | |
|---|---|---|---|---|---|---|
| | Polarization (VH) | Overall accuracy (%) | Kappa coefficient | Polarization (VV) | Overall accuracy (%) | Kappa coefficient |
| Sites 1 | 87.91 | 98.28 | 0.88 | 67.09 | 97.47 | 0.68 |
| Sites 2 | 127.21 | 96.74 | 0.92 | 94.76 | 94.18 | 0.70 |
| Sites 3 | 187.01 | 98.39 | 0.74 | 160.88 | 97.19 | 0.17 |
| Sites 4 | 233.25 | 98.61 | 0.77 | 210.13 | 98.80 | 0.76 |
| Total | 635.38 | 98.56 | 0.91 | 532.86 | 96.77 | 0.79 |

**Fig. 3** Comparison of VH and VV polarization showing variation of filter image

capable of reading, pre-processing, and visualizing Sentinel-1 SAR images. Digital imaging of satellite data was done using the ERDAS IMAGINE (2014) software, and editing of spatial information and map export was done using the ArcGIS (v.10.4.1) (Table 2).

## Methods

### SAR pre-processing

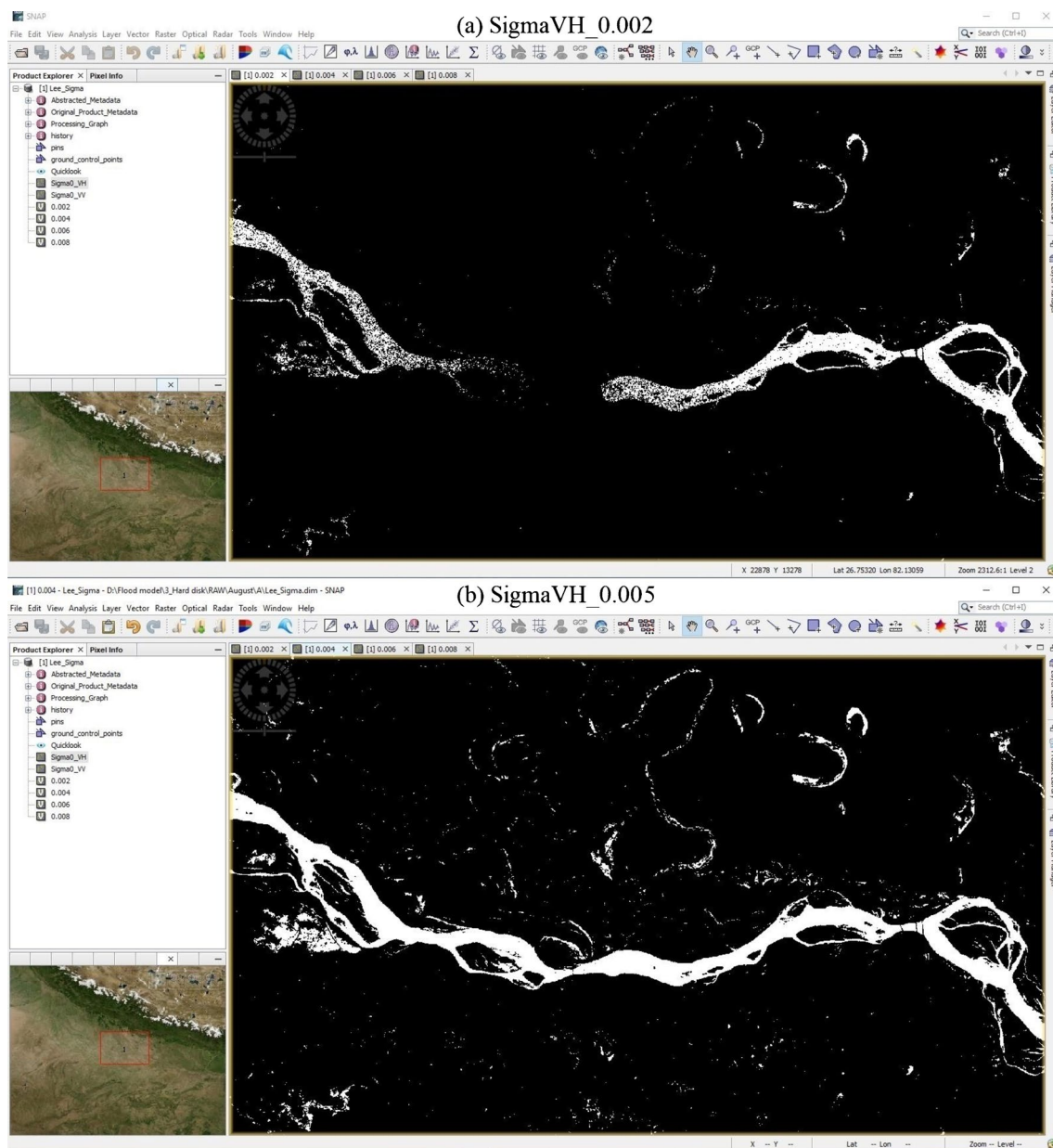In Sentinel-1 pre-processing, level-1 images were imported into the SNAP desktop tool. Sentinel-1A Level

**Fig. 4** Band math expression

1 GRD products require calibration to obtain backscattering values of objects on the Earth's surface, which is available free of charge from the website of the European Space Agency (ESA). The calibration is performed using the SNAP software. The first procedure to be performed when calibrating is to invoke the Orbit File application. The Apply Orbit file serves to correct and expand the orbit state vector containing information about the position and speed of the satellite motion direction, where the data is automatically downloaded when the process is executed (European Space Agency 2017). This is followed by thermal noise removal, radiometric calibration,

speckle filtering, and radiometric terrain correction (Small 2011; Pham-Duc et al. 2017). Ascending and descending data sets have been used for regular monitoring of floodplains. Following this, the polarization, band math expression has been applied to the SAR datasets (Fig. 2). Radiometric thermal noise due to satellite-generated heat has to be removed, especially when the intensity of the backscattered radar signal is low, which can cause image blur. The radiometric calibration is performed on a sigma naught backscattering model, where the model represents backscattering from the land surface (Atwood et al. 2012; Small 2011). Third, calibration for "VV and VH"

**Fig. 5** Sentinel-1 (VH polarization)
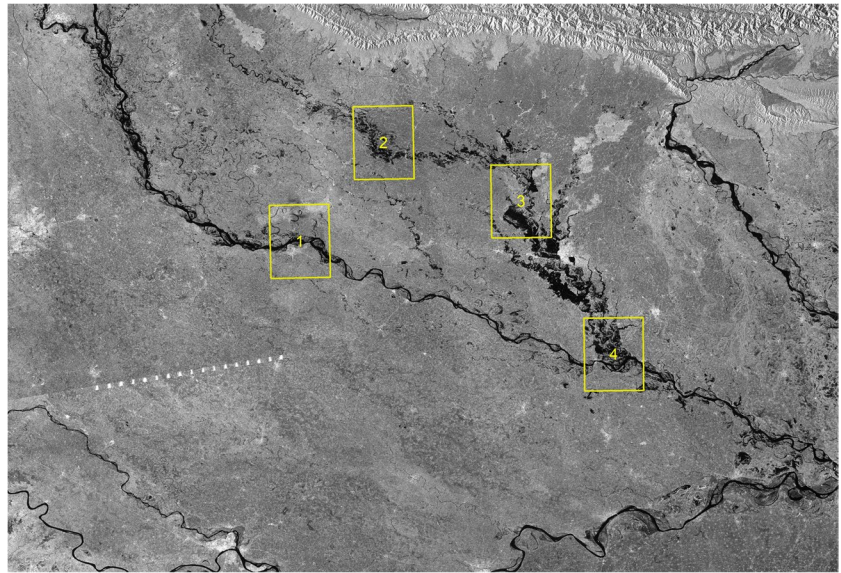


polarization is performed, after which the new product of backscatter coefficients is obtained. On flat areas, the surface acts as mirror; hence, wave beam reflected has no return energy strong enough to generate accurate radar image. Hence, identical scattering causes "false positives." Turbulent water shows signal returns; then, it can be considered a rough surface. This anomaly is mainly seen in fast flowing rivers which mark the degradation of the land surface. Speckle filter is applied to reduce the granular noise characteristic in SAR data. This gives smoothness without causing any loss to image details. SAR image products have distinctive features in the image display in the form of random dark and bright spots called speckles (Lillesand et al. 2015). This speckle is caused by constructive or destructive interference of the waves received by the SAR sensor which strengthens or weakens the value of pixel speckle (Lillesand et al. 2015; Jensen 2007). The algorithm used in this study is Lee's algorithm (Lee 1981).

Other than geometric distortion, there will be grainy noises appears in the image called speckle, which shall be filtered. The scattering intensity in a SAR image follows an exponential distribution.

$$pdf\left(^I/_{\sigma^0}\right) = \frac{1}{\sigma^0}\exp\left\{-\frac{1}{\sigma^0}\right\} \qquad (1)$$

where image intensity in a pixel is given by $I = Re\{U\}^2 + Im\{U\}^2$. The percentage of incoming radar energy scattered back to the sensor by an object on the ground is represented as $\sigma^o$. The speckle distribution pdf ($I/\sigma^o$) is plotted for three different $\sigma^o$ values. The speckle distribution becomes wider with increasing $\sigma^o$ and starts to approximate a uniform distribution for very high $\sigma^o$.

By considering the topography and geometry of the study areas, the polarization with low intensity values like the Lee filter along with window size $3 \times 3$ and $5 \times 5$ m, refined Lee and Lee sigma filter in which Lee sigma was chosen to be most appropriate for the study. Geometric and radiometric terrain correction is required to convert the coordinates of the sensor into map coordinates in remote sensing imagery to reduce geometric distortion (Shimada 2010). The SAR
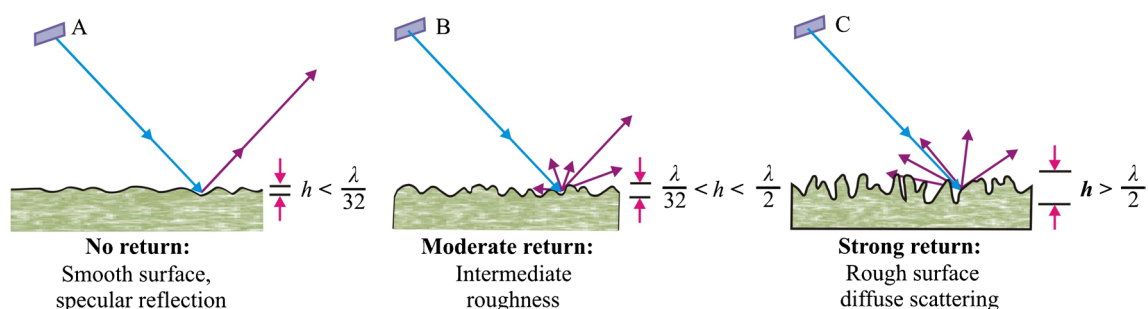


**Fig. 6** Conceptual drawing of the dependence of surface roughness on the sensor wavelength $\lambda$: **A** smooth surface, **B** intermediate surface, and **C** rough surface
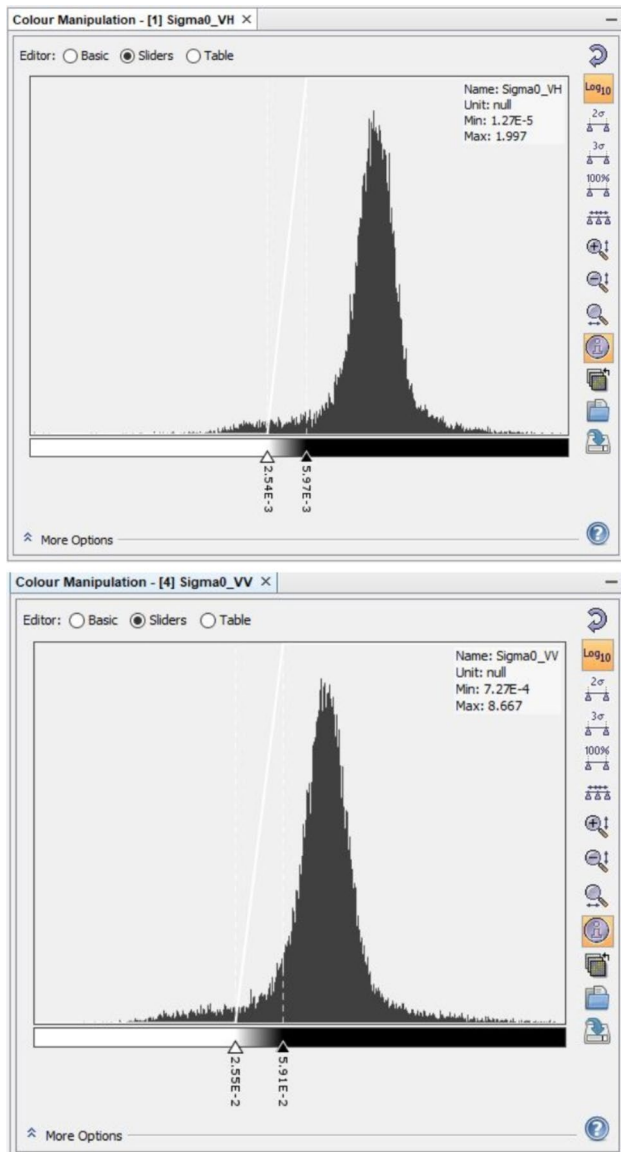
**Fig. 7** Histogram indicating the threshold used to retrieve flood extent of VH and VV polarizations

Simulation Terrain Correction algorithm in the SNAP software is used for geometric terrain correction processing of Sentinel-1 data, in which geometric distortions are corrected by transforming the coordinates to a standard reference frame. The ratio VH/VV is generated by dividing the band VH by the band VV. SAR images have geometric and radiometric distortion. The geometric mis-location of pixels occurs in topographically inclined areas, and the oblique angle of the illuminating radar energy induces topographic shading to the true surface RCS, giving radiometrically overexposed appearance, and leads to classification errors if images with different observation geometries are combined. The RCS of a pixel in a calibrated SAR image is composed of.

$$\sigma = \sigma^0(\theta_i)A_\sigma(\theta_i) \tag{2}$$

where $\sigma^o$ is normalized RCS, $\theta_i$ is the local incidence angle, and $A_\sigma$ is the surface area covered by a pixel. To retrieve the true RCS of the imaged surface ($\sigma^o$) from the observed radar data $\sigma$, the geometry dependence of $\sigma$ needs to be removed by correcting for $A_\sigma(\theta_i)$. The process of correcting for $A_\sigma(\theta_i)$ is called radiometric terrain correction (RTC). RTC removes geometry-dependent radiometric distortions corresponding to a pixel-by-pixel estimation and does compensation of $A_\sigma(\theta_i)$ on a DEM. The multi-look processing was carried out to reduce the speckle noise dB and improve image interpretability (Ganji et al. 2019).

## Threshold method

For the extraction of flood area, band math of value 0.005 is taken into consideration which gives a raster output showing flood area precisely. Sigma value 0.002 has poor ability to capture the amount of water, while 0.005 is good at capturing it accurately. Therefore, in the band math expression box, we use the formula (*if Sigma0_VH < 0.005, then 2 else 0*) for the qualitative result.

## Image processing

The second step is to extract the group merge value of the "flooded image" and radar backscatter, after which (band math equations) an algorithm of binary selects whether a pixel of the given raster is flooded or not (Aldhshan et al. 2019). Low values of the backscatter matched to the water, and high values matched to the non-water class. The final result was a grayscale image containing single band continuous data that generated from math band way using this formula: *255 * (single band < number color of grayscale).* After that, extraction of water body in ArcMap toolbox is carried out (Fig. 2).

## Result

Sentinel 1 SAR technique has played an important role in identifying flood waters along the major rivers of Uttar Pradesh. Table 2 provides measurements of the total flooded area in different areas of the SAR image, along with the surface area of the digitized polygons. The flood-induced area in the months of July, August, September, and October has been calculated as 1241, 4935, 3828, and 3909 km$^2$, respectively. The statistical analysis is based on the results of classified and photo-interpretation flood areas (Table 3). The total flood affected area along the river is 7710 km$^2$ in four months (Table 3). Spatially, maximum inundation is effective between elevations of 47–126 m above mean sea

**Fig. 8** Flood water classified in VH and VV polarizations
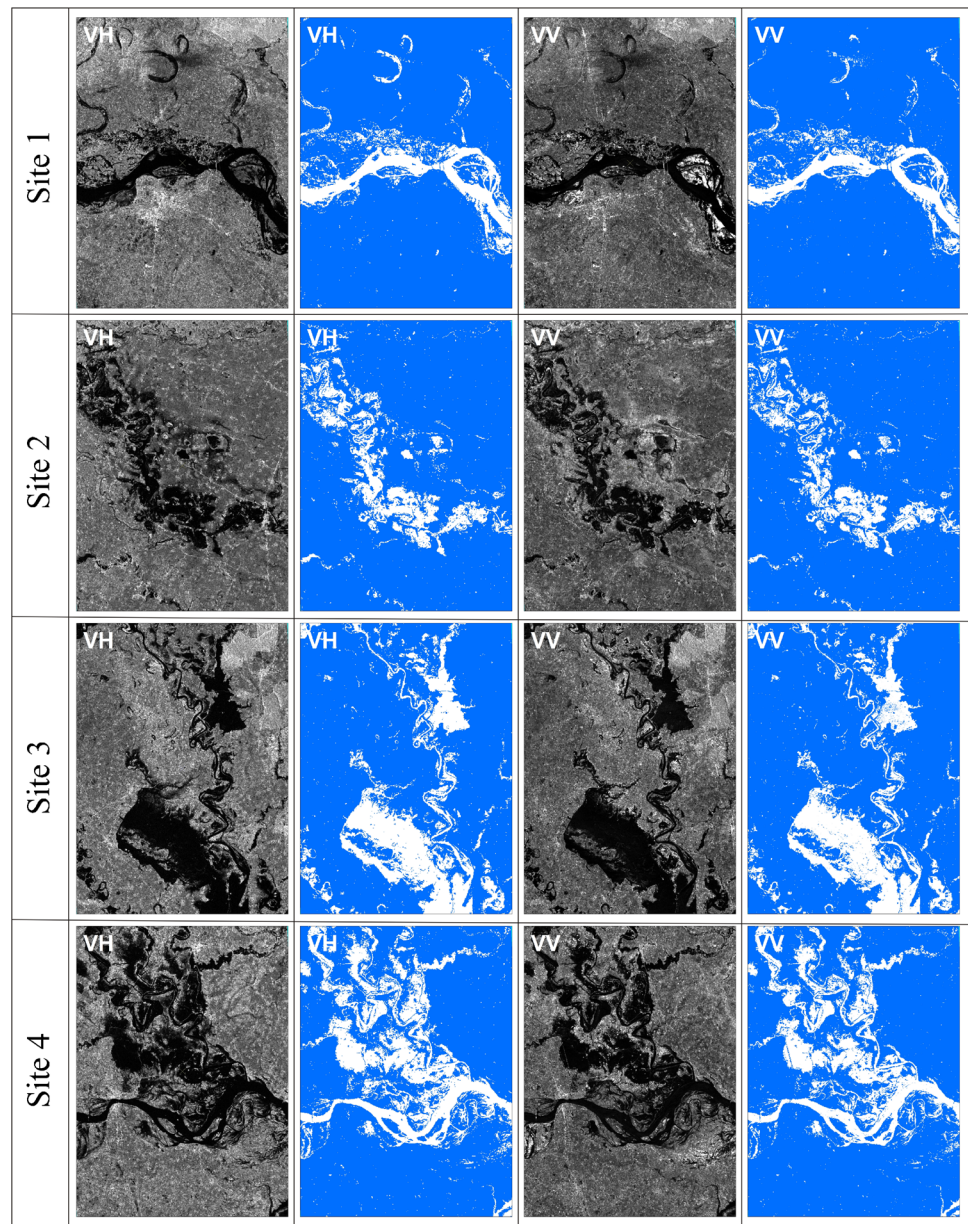


level. The comparison of flood extent in dual polarized data and digitized polygons shows that the total of flooded area for the five sites in the upstream of the Uttar Pradesh in the VH polarization is 635.38 ha, whereas in the VV polarization, it is estimated to be 532.86 ha (Table 4).

## Discussion

Li filter has been applied to both polarizations VV and VH before image processing of Sentinel-1 data to reduce random speckle noise (Lee et al. 1994; Henry 2004).

This filter generates different data more smoothly and minimizes loss of radiometric and textual information in image. A visual comparison of filters like refined Lee, Lee $3 \times 3$, Lee $5 \times 5$, and Lee Sigma has been done for areas like flood, urban, and crop (Fig. 3). The refined Lee filter gives smooth textured images with minimal radiometric and textural losses (Park et al. 2007; Ezzine et al. 2018; Fan and Lei 2012). Lee filter applies statistical parameters such as mean and standard deviation for window sizes $3 \times 3$ and $5 \times 5$, for smoothing. The standard "Lee Sigma" speckle filter and compared with the other speckle filters within Sentinel-1 Toolbox. Lee Sigma is preferred as it gives better results than others (Lee and Pottier 2009; Jaybhay 2015; Singh and Shree 2016). The Lee Sigma filter uses statistical analysis of digital values chosen by the operator and estimates the pixels accordingly (ESA Sentinel Online 2019).

**Fig. 9** Digitization of flood area
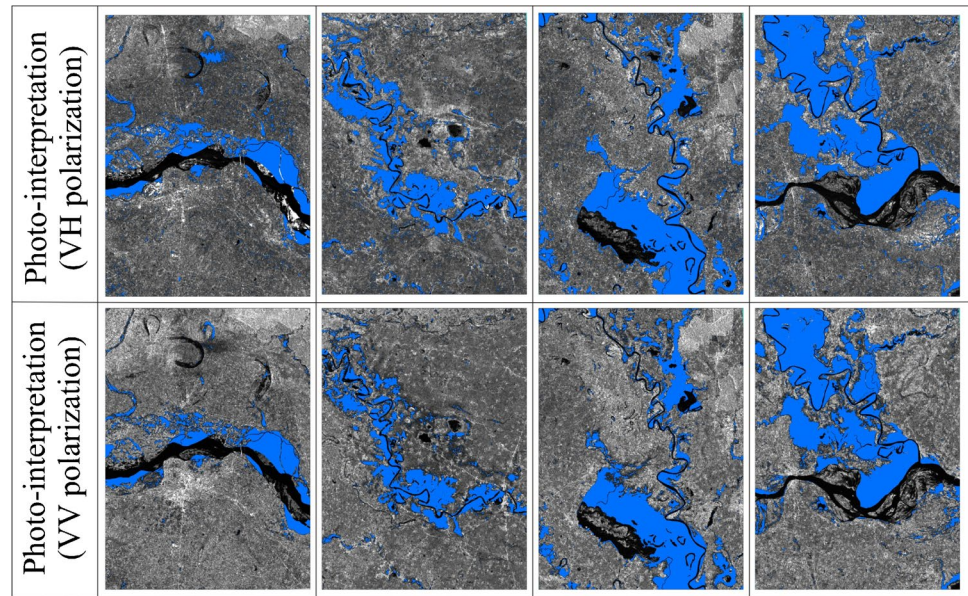


Backscattering analysis will demonstrate the water body and flood extended areas, and hence, a threshold value of (0.005) has been considered to find the optimum flood zone. The sigma value 0.002 has less capability of capturing the water content, while 0.005 is good at capturing it accurately. Therefore, in the band math expression box, we use the formula (if Sigma0_VV < 0.005, then 2 else 0) for the qualitative result (Fig. 4).

A site in the Sentinel-1 image has been selected to analyze and compare VH and VV polarizations along the classified flood zone. The VH polarization be revealed the most favorable results in both VV and VH which indicates the highest contrast. The submergence area includes rivers and floods in Uttar Pradesh. Four sites are selected in the Sentinel-1 image to analyze and compare VH and VV polarizations along the classified flood zone (Fig. 5). Backscattering of the SAR-transmitted signal is particularly sensitive to surface moisture and dielectric properties and roughness (Baghdadi et al. 2001).

According to Fig. 3, the backscatter signal of the water Sentinel-1 data is usually very low which means that the water acts as a specular reflective surface; it means a reflection off a smooth surface in which the angle of incidence ($i$) equal the angle of reflection ($r$) (Fig. 6A). Therefore, appearing black in SAR images compared to the backscatter signals from other surfaces such as rough surface, it means scattering off a rough surface; the variation in surface height is on the order of the magnitude of the wavelength on the incoming signal (Fig. 6B) and multiple scattering or volume scattering on vegetation can strongly influence the brightness of the SAR image such as vegetation (Fig. 6C) which means signal scattered in many directions (Lei 2016).

The threshold technique is used to separate flooded areas from non-flooded areas. This method has been praised for its simplicity and short processing time (Brivio et al. 2002; Henry et al. 2006; Martinis et al. 2010; Zwenzner 2009). Basically, after analysis of the backscatter, histogram of the image pixels with intensity lower than a defined threshold is considered flooded while pixels with higher backscatter are considered not flooded. To correct this threshold, the low backscattering of water bodies, at the surface where specular reflection predominates, is often used to easily distinguish them from other types of land cover (Martinis 2010; Martinis et al. 2010). To identify the water boundary on filtered VV and VH polarization, we chose an approach based on automatic threshold.. This threshold is determined by establishing a histogram of the data (Fig. 7). The threshold method, applied on VV polarizations, reveals flaws in the observation of flooded affected region compared to VH polarizations delineating flood. The resulting comparison shows that there is a considerable difference in the flood area. The VH polarization can better identify water from land. The resulting comparison in this study shows considerable variation in flood zones. The visual interpretation between VH and VV polarization and the corresponding classified water shows that in VH-polarized data. The intensity of flood has been measured higher in site 4, while lowest in site 1 due to variation in slope and confluence of Ghaghara and Rapti River. Therefore, the flood area extracted from VH polarization is more than that of VV polarization (Fig. 8; Table 4). The photo-interpretation technique comprises in digitizing flooded areas in VH and VV polarization. The results can therefore be validated by comparing the water surfaces extracted from the digitized polygons of the VH and VV maps (Fig. 9).
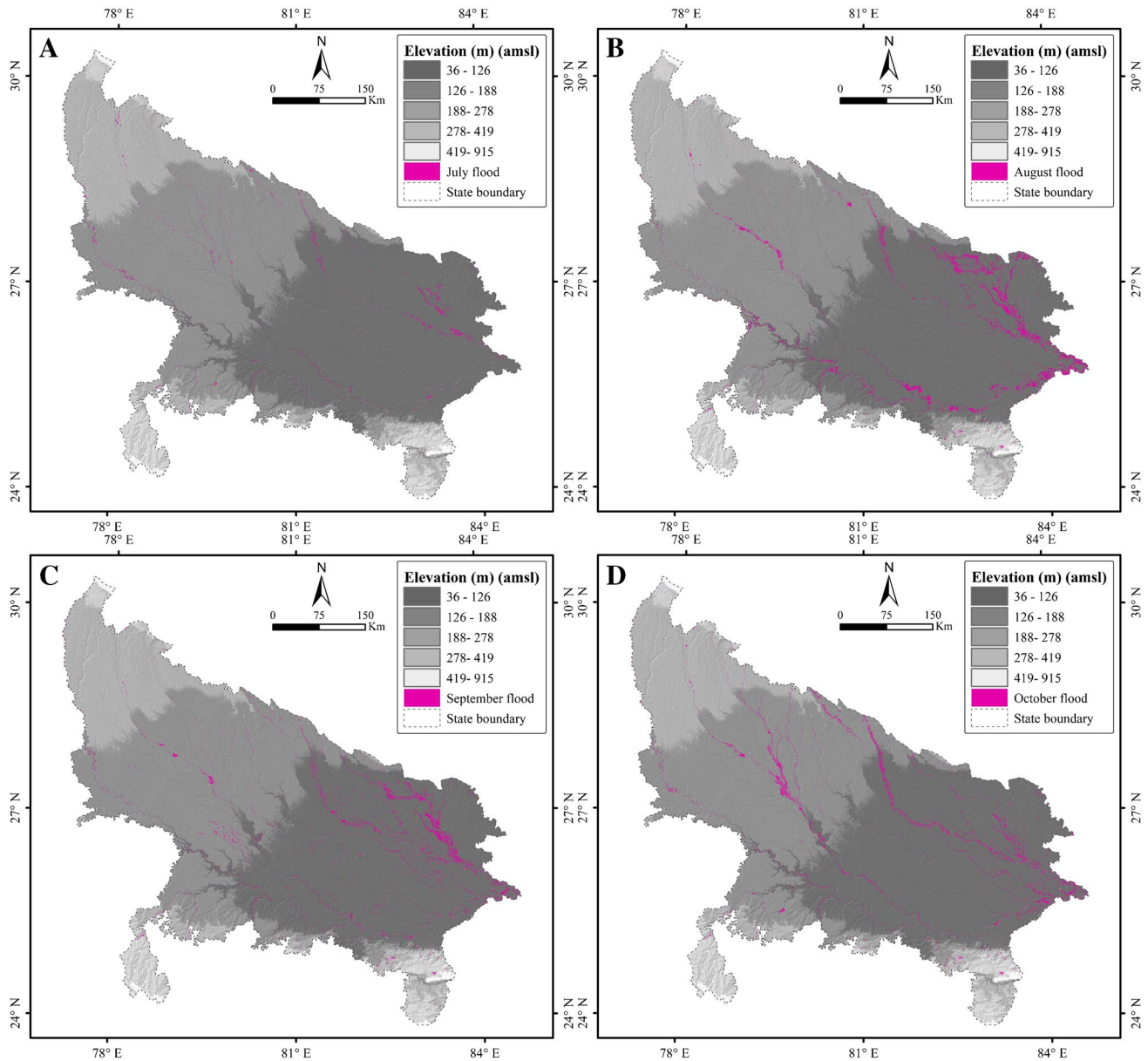
**Fig. 10** **A** Flood inundated area during July, **B** flood inundated area during August, 2021, **C** flood inundated area during September, and **D** flood inundated area during October, 2021

Temporally, the maximum flood during the overall rainfall period occurred in the month of August. The monsoon commences by the end of June in Uttar Pradesh, slightly increasing from July. During August, shallow areas and dry channels are filled, and significant floods occur along the major river. The monsoon decreased over the UP in September, followed by submergence in several low-lying areas. In October, the dry channel submerges in some areas, while the flood recedes as rainfall decreases at other places (Fig. 10).

Backscattering of the SAR-transmitted signal is especially sensitive to surface moisture and its dielectric properties and roughness (Baghdadi and Chaaya 2011). The results showed the accurate floodplains along the rivers of Uttar Pradesh during monsoon season, in 2021 (Fig. 11). Photo-interpretation analysis revealed that the flood area distinguish in VH images is more important than the flood surfaces in VV images. This suggested that flood area in the Uttar Pradesh would be easier to identify with VH data rather than with VV. In addition, the Kappa coefficient and the overall accuracy parameter used to estimate the performance of VH and VV images in the classification of submerged areas. Math using the confusion matrix of these coefficient polarization

**Fig. 11** Flood inundated area along Ghaghara River and Rapti River in Uttar Pradesh
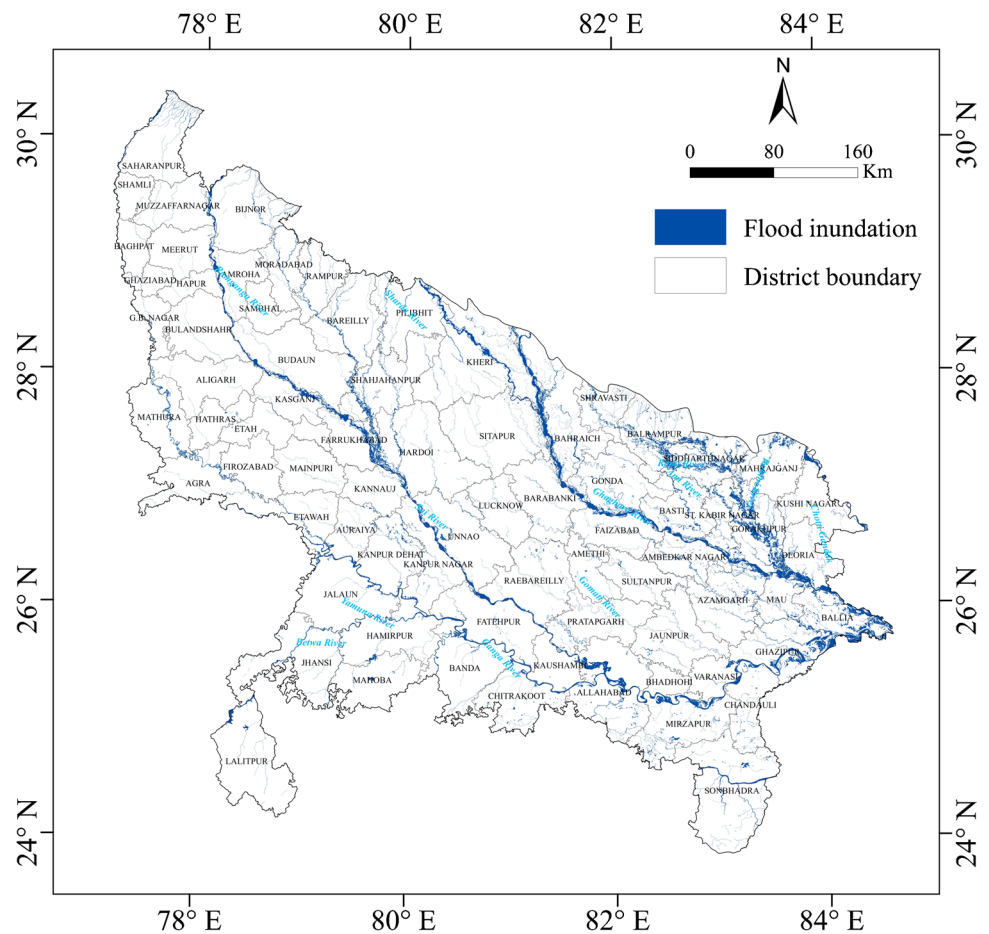


data and photo-interpretation images of VH and VV shows that VH image rapidly recognizes large. The ratio of submerged area to VV is shown in Table 4. This examination tends to confirm that VH polarization is more efficient for delineating flooded areas.

### Significance of the study

The method proposed in this paper has been used to detect flood inundation region with optimized algorithms and synthetic aperture radar (SAR) techniques. It is a comprehensive and effective way of providing accurate surface water information, rapid and accurate flood assessment instead of the traditional method of flood mapping. There has been an important contribution of space technology in the preparedness, prevention, and relief phases of flood disaster management. RS technologies have made it easier to map large areas under flood and provide early warning of disaster which can help in providing assistance and reducing damage in crisis situations. Using datasets and models, future work on disasters like floods can be done through microwave technology. Sentinel 1A images have been used to map and identify flood-prone areas of Uttar Pradesh. It will be used to detect

changes in flood-prone areas and potential flood encroachment as well as to aid decision making during disasters.

### Conclusions

1. Sentinel-1 data allows us to easily differentiate between surface and water on land, which enables mapping of water boundaries. SAR images were subjected to various processes of correcting and filtering like orbital parameters, radiometric, noise reduction speckle, and geometric correction. The study aims flood monitoring during the monsoon season of 2021 along the major river of Uttar Pradesh with the help of Sentinel 1A SAR microwave data. Ascending and descending data sets has acquired to obtain for regular monitoring of flood regions. VH shows the most promising results in both the polarization VV and VH by demonstrating the highest contrast. Speckle reduction technique Lee $5 \times 5$ does reduce the resolution quality but helps in reducing the false positive.

2. The study aims to flood monitoring during the monsoon season of 2021 along the major river of Uttar Pradesh

with the help of Sentinel 1A SAR microwave data. Ascending and descending data sets have been acquired to obtain for regular monitoring of flood regions.

3. On performing the analysis, the total flood inundated area extracted is 7710 $km^2$. Temporally, the maximum flood during the overall rainfall period occurred in the month of August. Spatially, the maximum flood is dominant in elevation between 47 and 126 m (AMSL).

4. On application of DEM, it is found that the flooding is mainly affected by the terrain. In this study, the submerged and flood inundated area, monsoon intensity, and impact of the river and spatial extent of the flood were identified.

5. This study confirmed the capability of this sensor to produce flood maps. We also highlight that while the VH polarization better identifies the flooded regions, the flooding in the VH polarization is larger than that in the VV polarization. The data has been compared with the inundation area obtained from the digitized polygons. The results show that Sentinel-1's VH data is sufficient for flood detection as compared to VV. VH shows the most promising results in both the polarization VV and VH by demonstrating the highest contrast. Therefore, VH polarization has greater efficiency in better-identifying flood areas.

6. The results show the importance of rapid and easy extraction of the data in the form of imageries and how it helps in predicting the flood behavior. The new set of data shall be used in development of hydrological models and for accurately predicting and warning in case of future flood disasters. In the future, we plan to expand the dataset and test the model in more complex scenarios to further improve the performance and applicability. This study may provide a new idea and method for microwave detection of water bodies.

**Data availability**  Data is available on request.

## Declarations

**Competing interests**  The authors declare no competing interests.

## References

Abazaj Hasko G (2020) Use of Sentinel-1 data in flood mapping in the Buna River area. Int J Environ Climate Change 10(10):147–156

Adelekan I (2011) Vulnerability assessment of an urban flood in Nigeria, Abeokuta Flood 2007, 56th edition. Nat Hazards 56:215–231

Aldhshan SR, Mohammed OZ, Shafri HM (2019) Flash flood area mapping using sentinel-1 SAR data: a case study of eight upazilas in Sunamganj district, Bangladesh. IOP Conf Ser Earth Environ Sci 357:012034. https://doi.org/10.1088/1755-1315/357/1/012034

Amitrano MD, Iodice A, Riccio D, Ruello G (2018) Unsupervised rapid flood mapping using Sentinel- 1 GRD SAR images. IEEE Trans Geosci Remote Sens 56(6):3290–3299

Atwood K, David S, Gens R (2012) Improving PolSAR land cover classification with radiometric correction of the coherency matrix. IEEE J Select Appl Earth Observ Remote Sens 5(3):848–857

Baghdadi JA, Chaaya MZ (2011) Semiempirical calibration of the integral equation model for SAR data in C-band and cross polarization using radar images and field measurements. IEEE Geosci Remote Sens Lett 8:14–18

Baghdadi N, Bernier M, Gauthier R, Neeson I (2001) Evaluation of C-Band SAR-Data for wetlands mapping. Int J Remote Sens 22(1):71– 88. https://doi.org/10.1080/014311601750038857

Bhatt CM, Rao GS, Begum A, Manjusree P, Sharma SV, Prasanna L, Bhanumurthy V (2013) Satellite images for extraction of flood disaster footprints and assessing the disaster impact: Brahmaputra floods of June–July 2012, Assam, India. Curr Sci 104(12):1692–1700

Bolanos SD, Brisco B, Pietroniro A (2016) Operational surface water detection and monitoring using Radarsat. Remote Sens 8(4):285

Brivio CR, Maggi M, Tomasoni R (2002) Integration of remote sensing data and GIS for accurate mapping of flooded areas. Int J Remote Sens 23:429–441

Chutiya D, Hazarika N, Das P (2009) Adjusting to floods on the Brahmaputra Plains. Assam, India. International Centre for Integrated Mountain Development (ICIMOD), Kathmandu, Nepal

Demir V, Kisi O (2016) Flood hazard mapping by using geographic information system and hydraulic model: Mert River, Samsun, Turkey. Adv Meteorol 2016:489–1015

ESA Sentinel Online (2019) User guides and technical guides of Sentinel-1 SAR

European Space Agency (2016) Sentinel-1 product definition. European Space Agency

European Space Agency (2017) Sentinel-1 Toolbox (S1TBX), version 6.0.0–20170802

Ezzine DF, Rajhi H, Ghatassi A (2018) Evaluation of Sentinel-1 data for flood mapping upstream Sidi Salem dam (Northern Tunisia). Arab J Geosci 11:170

Fan JL, Lei B (2012) A modified valley-emphasis method for automatic Thresholding. Pattern Recogn Lett 33(6):703–708

Gautam PK (2023a) The significance of morphometric analysis of Shimsha River, Karnataka, India to understand the hydrological and morphological characteristics. River 2(4):490–505. https://doi.org/10.1002/rvr2.66

Gautam PK (2023b) Sedimentology of the lower part of Ghaghara River basin from Faizabad to Deoria in Ph.D. Thesis. Geology Department, Lucknow University, Lucknow, India, pp 55–57

Gautam PK, Singh DS (2022) Flood hazard and risk assessment of Deoha River Basin. Central Ganga Plain-India, GIS approach. Disaster Adv 15(10):42–51

Gautam PK, Singh AK (2023) Evaluation of active tectonic features of nandakini river basin lesser himalaya india by using morphometric indices: a GIS approach. Adv Environ Eng Res 04(01):1–24. https://doi.org/10.21926/aeer.2301014

Ganji K, Gharachelou S, Ahmadi A (2019) Urban's river flood analysing using sentinel-1 data case study: (gorganrood, aq'qala), Int Arch Photogramm Remote Sens Spatial Inf Sci XLII-4/W18 415–419. https://doi.org/10.5194/isprs-archives-XLII-4-W18-415-2019

Gautam PK, Singh DS, Kumar D, Singh AK (2020) A GIS based approach in drainage morphometric analysis of Sai River Basin, Uttar Pradesh, India. J Geol Soc India 95:366–376

Gautam PK, Singh DS, Kumar D, Singh AK, Vishawakarma B (2022a) Assessment of morphometric characteristics and decadal fluctuation of groundwater level of Kali River basin and its link with climate change, West Indo-Gangetic plain of India Using Geographical Information System. Disaster Adv 15(5):26–38

Gautam PK, Singh DS, Singh AK, Kumar D (2022b) Geomorphic analysis of Baghain River, Yamuna Basin, and its implication for drainage characteristic and tectonics using remote sensing and GIS techniques. J Geol Soc India 98:1573–1584

Gautam PK, Kumar D, Singh AK, Singh DS (2023) Drainage network analysis and tectonics interference of the Reth River, Central Ganga Plain (India) using geospatial technology. Geotectonics 57(3):330–345

Greifeneder WW, Sabel D, Naeimi V (2014) Suitability of SAR imagery for automatic flood mapping in the Lower Mekong Basin. Int J Remote Sens 35(8):2857–2874

Henry JB (2004) Systèmes d'information spatiaux pour la gestion du risque d'inondation de plaine Thèse De Doctorat, Géographie Physique, Université De Strasbourg I 192

Henry CP, Fellah K, Desnos YL (2006) ENVISAT multi-polarised ASAR data for flood mapping. Int J Remote Sens 27:1921–1929

Jain V, Sinha R (2003) River systems in the Gangetic plains and their comparison with the Siwaliks. A review. Curr Sci 84(8):1025–1033

Jaybhay Shastri R (2015) A study of speckle noise reduction Filters Signal & Image Processing. An Int J (SIPIJ) 6(3):71–80

Jensen JR (2007) Remote sensing environment: an Earth resource perspective, 2nd edn. Pearson Education Inc., United States of America

Joyce Belliss SE, Samsonov SV, Mcneill SJ, Glassey PJ (2009) A review of the status of satellite remote sensing and image processing techniques for mapping natural hazards and disasters. Prog Phys Geogr Earth Environ 33(2):183–207

Karamvasis KV (2021) FLOMPY: an open-source toolbox for flood-water mapping using Sentinel-1 intensity time series. Water 13(21):2943

Khan S, Sinha R, Whitehead P, Sarkar S, Jin L, Futte MN (2018) Flows and sediment dynamics in the Ganga River under present and future climate scenarios. Hydrol Sci J 63:763–782

Kumar S, Singh IB (1978) Sedimentological study of Gomati River sediments, Uttar Pradesh, India. Example of a river in alluvial plain 145–211

Kumar D, Singh DS, Prajapati SK, Khan I, Gautam PK, Vishawakarma B (2018) Morphometric analysis of Kalyani River Basin, Ganga Plain, a remote sensing and GIS approach. J Geol Soc India 91:679–686

Kumar D, Singh AK, Gautam PK, Vishawakarma B, Dubey CA, Singh DS (2024) Response of global warming on glaciers of Garhwal Himalaya, India a remote sensing and GIS approach. In: Khare N (ed) Polar ice and global warming in cryosphere regions. Taylor and Francis (CRC Plus), (5):91–107

Lee JS (1981) Speckle analysis and smoothing of synthetic aperture radar images. Comput Graphics Image Process 17(1):24–32

Lee JS, Pottier E (2009) Polarimetric radar imaging: from basics to applications. In Optical Science and Engineering. CRC Press, Boca Raton, FL, USA, p 142

Lee JS, Jurkevich I, Dewaele P, Wambacq P, Oosterlinck A (1994) Speckle filtering of synthetic aperture radar images. A review. Remote Sens Rev 8:313–340

Lei Y, Siqueira P, Treuhaft R (2016) A dense medium electromagnetic scattering model for the InSAR correlation of snow. Radio Sci 51:461–480. https://doi.org/10.1002/2015RS005926

Li Y, Martinis S, Wieland M, Schlaffer S, Natsuaki R (2019) Urban flood mapping using SAR intensity and interferometric coherence via Bayesian network fusion. Remote Sens 11(19):2231

Lillesand M, Kiefer RW, Chipman JW (2015) Remote sensing and image interpretation, Seventh. John Wiley & Sons Inc., United States of America

Long S, Fatoyinbo TE, Policelli F (2014) Flood extent mapping for Namibia using change detection and thresholding with SAR. Environ Res Lett 9(3):035002

Luo T, Maddocks A, Iceland C, Ward P, Winsemius H (2015) World's 15 countries with the most people exposed to river floods. World Resources Institute: Washington, DC, USA 5

Manavalan (2017) SAR image analysis techniques for flood area mapping literature survey. Earth Sci Inf 10(1):1–14

Manjusree P et al (2012) Optimization of threshold ranges for rapid flood inundation mapping by evaluating backscatter profiles of high incidence angle SAR images. Int J Disaster Risk Sci 3:113–122

Martinis S (2010) Automatic near real-time flood detection in high resolution X-band synthetic aperture radar satellite data using context-based classification on irregular graphs. PhD thesis. University of Munchen

Martinis S, Twele A, Voigt S (2010) Towards operational near real-time flood detection using a split-based automatic thresholding procedure on high resolution Terra SAR-X data. Nat Hazard 9:303–314

Martinis S, Jens K, André T (2015) A fully automated TerraSAR-X based flood service. ISPRS J Photogramm Remote Sens 104:203–212

Mason DC, Davenport IJ, Neal JC, Schumann GJP, Bates PD (2012) Near real-time flood detection in urban and rural areas using high-resolution synthetic aperture radar images. IEEE Trans Geosci Remote Sens 50:3041–3052

Meyer WZ, Kragh SJ, Andreasen M, Jensen KH, Fensholt R, Looms MC (2022) Exploring the combined use of SMAP and Sentinel-1 data for downscaling soil moisture beyond the 1 km scale. Hydrol Earth Syst Sci 26(13):33–37

Milliman JD, Farnsworth KL (2011) River discharge to the coastal ocean. Cambridge University Press, New York, NY, USA

Nandargi SS, Shelar A (2018) Rainfall and flood studies of the Ganga River Basin in India. Annals of Geographical Studies 1(1):34–50

Nasirzadehdizaji R, Sanli FB, Abdikan S, Cakir Z, Sekertekin A, Ustuner M (2019) Sensitivity analysis of multi-temporal sentinel-1 SAR parameters to crop height and canopy coverage. Appl Sci 9:655

Ogah AT, Abiola KA, Magaji JI, Ijeogu EO, Opaluwa OD (2013) Flood risk assessment of river Mada: a case study of Akwanga local government area of Nasarawa state. Nigeria Adv Appl Sci Res 4(1):407–416

Park JM, Song WJ, Pearlman WA (2007) Speckle filtering SAR images based on adaptive windowing. IEEE Proc Vis Image Signal Process 146:191–197

Patel P, Srivastava HS, Navalgund RR (2009) Use of synthetic aperture radar polarimetry to characterize wetland targets of Keoladeo National Park, Bharatpur India. Curr Sci 97(4):529–537

Perucca LP, Angilieri YE (2010) Morphometric characterization of delMolle Basin applied to the evolution of flash floods hazards Iglesia Department, San Jaun, Argentina. Quarternary Internat 233(1):81–86

Pham-Duc B, Aires Prigent C, F, (2017) Surface water monitoring within cambodia and the Vietnamese Mekong Delta over a year, with Sentinel-1 SAR observations. Water 9(6):1–21

Pradhan B, Tehrany MS, Jebur MN (2016) A new semiautomated detection mapping of flood extent from terrasar-x satellite image using rule-based classification and taguchi optimization techniques. IEEE Trans Geosci Remote Sens 54:4331–4342

Rahman R, Thakur PK (2017) Detecting, mapping and analyzing of flood water propagation using synthetic aperture radar (SAR) satellite data and GIS: a case study from the Kendrapara district of Orissa state of India. Egypt J Remote Sens Space Sci 21

Rahman R, Thakur PK (2018) Detecting, mapping and analyzing of flood water propagation using synthetic aperture radar (SAR) satellite data and GIS: a case study from the Kendrapara District of Orissa State of India. Egypt J Remote Sens Space Sciences 21:37–41

Rudra K (2014) Changing river courses in the western part of the Ganga-Brahmaputra delta. Geomorphology 227:87–100

Sahoo SN, Sreeja P (2017) Development of flood inundation maps and quantification of flood risk in an urban catchment of Brahmaputra River. ASCE-ASME J Risk Uncertain Eng Syst Part A Civ Eng 3(1):A4015001

Sezgin M, Sankur B (2004) Survey over thresholding techniques and quantitative performance evaluation. J Electron Imaging 13(1):146–165

Shimada M (2010) Ortho-rectification and slope correction of SAR data using DEM and its accuracy evaluation. IEEE J Select Topics Appl Earth Observ Remote Sens 3(4):657–672

Singh RL (1988) India: a regional Geography. National Geographical Society, India, Varanasi, India, p 992

Singh DS (2007) Flood mitigation in the Ganga Plain. In: Rai N, Singh AK (eds) Disaster management in India. New Royal Book Company, pp 167–179

Singh DS (2015) Climate change, past present and future. J Geol Soc India 85:634–635

Singh DS, Awasthi A (2011) Natural hazards in the Ghaghara River Area, Ganga Plain, India. Nat Hazards 57:213–225

Singh P, Shree R (2016) Analysis and effects of speckle noise in SAR images. In Advances in Computing, Communication, & Automation (Fall). ICACCA, pp 2–6

Singh DS, Awasthi A, Nishat R (2010) Impact of climate change on the rivers of Ganga Plain. Inter Jour Rur Devel Manag Stud 4(1):1–8

Singh DS, Prajapati SK, Kumar D, Awasthi A, Bhardawaj V (2013) Sedimentology and channel pattern of the Chhoti Gandak River, Ganga Plain, India. Gondwana Geol Magazine 2:171–180

Singh DS, Prashant SK, Singh P, Singh K, Kumar D (2015) Climatically induced levee break and flood risk management of the Gorakhpur region Rapti River basin Ganga Plain India. J Geol Soc India 85(1):79–86. https://doi.org/10.1007/s12594-015-0195-6

Singh S, Tiwari AB, Gautam PK (2018) Burhi Gandak River: the place of first republic of the world. The Indian Rivers: Scientific and Socio-Economic Aspects. 1st edt. Springer Hydrogeol 2:209–219

Singh DS, Dubey CA, Kumar D, Vishawakarma B, Singh AK, Tripathi A, Gautam PK, Bali R, Agarwal KK, Sharma R (2019) Monsoon variability and major climatic events between 25 and 0.05 ka BP using sedimentary parameters in the Gangotri Glacier region, Garhwal Himalaya, India. Quat Int 507:148–155. https://doi.org/10.1016/j.quaint.2019.02.018

Singh AK, Kumar D, Dubey CA, Gautam PK, Vishawakarma B, Singh DS (2022) Glacial morpho-sedimentology and processes of landscape evolution in gangotri glacier area, Garhwal Himalaya, India. In: Khare N, 1st ed. Taylor and Francis (CRC Press), 1:223–238. https://doi.org/10.1201/9781003284413

Sinha R, Tandon SK, Gibling MR, Bhattacharjee PS, Dasgupta AS (2005) Late quaternary geology and alluvial stratigraphy of the Ganga basin. Himalayan Geol 26(1):223–240

Sivasankar T, Das R, Borah SB, Raju P (2019) Insight to the potentials of Sentinel-1 SAR data for embankment breach assessment https://doi.org/10.1007/978-3-319-77276-9_4

Small D (2011) Flattening gamma: radiometric terrain correction for SAR imagery. IEEE Trans Geosci Remote Sens 49(8):3081–3093

Srivastava S, Patel P, Navalgund RR (2006) How far SAR has fulfilled its expectation for soil moisture retrieval. Proceeding: SPIE, pp 1–12

Tavus RC, Kocaman S (2022) A CNN-based flood mapping approach using SENTINEL-1 data. ISPRS Ann Photogramm Remote Sens Spat Inf Sci 3:549–556

Tavus E, Kocaman SU, Gokceoglu C, Nefeslioglu HA (2018) Considerations on the use of sentinel-1 data in flood mapping in urban areas: Ankara (Turkey) 2018 floods. International Archives of the Photogrammetry, Remote Sensing & Spatial Information Sciences

Torres R et al (2012) GMES Sentinel-1 mission. Remote Sens Environ 120:9–24

Uddin MA, Matin MFJ (2019) Operational flood mapping using multitemporal Sentinel-1 SAR images: a case study from Bangladesh. Remote Sens 11(13):1581

Uddin K, Matin MA, Meyer FJ (2019) Operational flood mapping using multi-temporal Sentinel-1 SAR images: A Case Study from Bangladesh. Remote Sens 11:1581

Valdiya KS (2004) Lessening the ravages of floods. book: Geology, environment and society. Universities Press, India, pp 112–115

Vanama SK, Musthafa M, Khati U, Gowtham R, Singh S, Rao YS (2021) Inundation mapping of Kerala flood event in 2018 using ALOS-2 and temporal Sentinel-1 SAR images. Curr Sci 120(5):915–925

Varnes DJ (1984) Landslide hazard zonation: a review of principles and practice. Unesco, Paris

Voormansik K, Praks J, Antropov O, Jagomagi J, Zalite K (2014) Flood mapping with terrasar-X in forested regions in Estonia. IEEE J Sel Top Appl Earth Obs Remote Sens 7(2):562–577

Wallemacq P, Guha-Sapir D, McClean D (2015) The human cost of weather-related disasters. Centre for Research On the Epidemiology of Disasters (CRED) United Nations Office for Disaster Risk Reduction 30

Zwenzner, Stefan V (2009) Improved estimation of flood parameters by combining space based SAR data with very high resolution digital elevation data. Hydrol Earth Syst Sci 13. 10.5194/hess-13-567